JOC The Journal of Organic Chemistry

Article

pubs.acs.org/joc

Boron Dipyridylmethene (DIPYR) Dyes: Shedding Light on Pyridine-Based Chromophores

Jessica H. Golden,[†] John W. Facendola,[†] Daniel Sylvinson M. R.,[†] Cecilia Quintana Baez,[‡] Peter I. Djurovich,[†] and Mark E. Thompson*[,†,‡]

[†]Department of Chemistry and [‡]Mork Family Department of Chemical Engineering and Materials Science, University of Southern California, Los Angeles, California 90089, United States

Supporting Information

ABSTRACT: Boron dipyrromethene (BODIPY) derivatives have found widespread utility as chromophores in fluorescent applications, but little is known about the photophysical properties of pyridine-based BODIPY analogues, dipyridylmethene dyes. Indeed, it has been reported that boron difluoride dipyridylmethene (DIPYR) is nonemissive, and that derivatives of DIPYR have modest, if any, luminescence. In this report, we explore this little-touched area of chemical space and investigate the photophysical properties of three simple DIPYR dyes: boron dipyridylmethene, boron diquinolylmethene, and boron diisoquinolylmethene. The three dyes strongly absorb in the blue-green part of the spectrum (λ_{em} = 450−520 nm, ε = 2.9−11 × 10^4 M^{-1} cm^{-1}) and display green fluorescence with high quantum yields (Φ_{PL} = 0.2, 0.8, and 0.8, respectively). Key photophysical properties in these systems were evaluated using a combination of TD-DFT and extended multiconfigurational quasidegenerate second-order perturbation theory (XMCQDPT2) methods and compared to experimental results, revealing that high quantum yields of the quinoline and isoquinoline derivatives are a result of the relative reordering of S_1 and T_2 state energies upon benzannulation of the parent structure. The intense absorption and high emission efficiency of the benzannulated derivatives make these compounds an intriguing class of dyes for further derivatization.

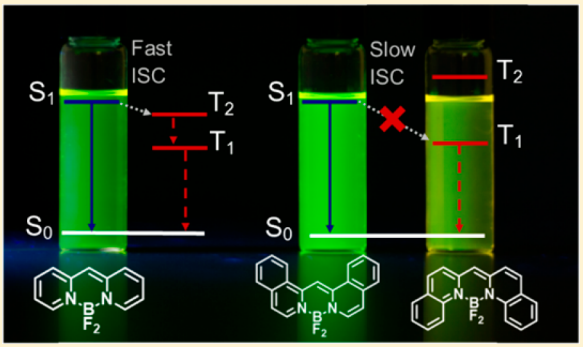

INTRODUCTION

The boron dipyrromethene (BODIPY) core structure is pervasive among fluorescent dyes employed in biological and optoelectronic applications. BODIPYs have been utilized in protein and DNA labeling,[1−5] as fluorescent switches and chemosensors,[6−8] as laser dyes,[9] and in photovoltaics.[10,11] Their physical and photophysical properties can be readily tuned by making simple substitutions on the pyrroles or at the *meso* position, and they tend to have little dependence on solvent polarity or pH, which makes them ideal fluorophores for *in vivo* labeling.[12] These features, along with a high luminance efficiency and photostability, have led to the popularity of BODIPY compounds. Despite the wide landscape of available BODIPY dyes, further investigation into the derivatization of BODIPYs and the development of alternative fluorescent dyes remain an active area of research because of specific limitations presented by BODIPYs.[13] Indeed, some simple synthetic modifications of BODIPYs have proven challenging; for example, although the class of dyes has been known since 1968, it was not until 2009 that the parent structure was successfully isolated.[14−16] Given the enormous available body of work on the derivatization and application of BODIPYs and related fluorophores, we found it surprising that very little research has been reported on the photophysical properties of pyridine-based BODIPY-like dyes.

In this work, we aim to expand the scope of BODIPY-like dyes by the replacement of the pyrroles in BODIPY with pyridine moieties. The resultant class of boron difluoride dipyridylmethene (DIPYR) fluorescent dyes (Figure 1) is similar in geometric structure to anthracene and dibenz[*a*,*j*]-anthracene, and superficially appears to be a mix between acenes and BODIPYs. Considering their intriguing combination of structural features, it is therefore somewhat surprising that only a handful of studies have appeared regarding the photophysical properties for this class of compounds. For example, the first report on the preparation of DIPYR in 1973 made no mention of luminescent properties,[17] while a later paper describing the photophysical properties of the related boron dipyridylamine dyes incorrectly described DIPYR as being nonemissive.[18] It is likely for this reason that follow-up research on this class of dye molecules has been limited.[19] However, dipyridylamine analogues of DIPYR dyes with nitrogen at the *meso* position do display UV−violet emission (λ_{em} = 362−416 nm) and have luminescent quantum yields (Φ_{PL} = 0.4)[18] that are similar to values found for the blue-emissive *meso*-cyano-substituted DIPYR dyes (λ = 450 nm, Φ_{PL} = 0.2).[19] These promising photophysical properties piqued

Received: April 5, 2017
Published: July 4, 2017

ACS Publications © 2017 American Chemical Society

DOI: 10.1021/acs.joc.7b00786
J. Org. Chem. 2017, 82, 7215−7222

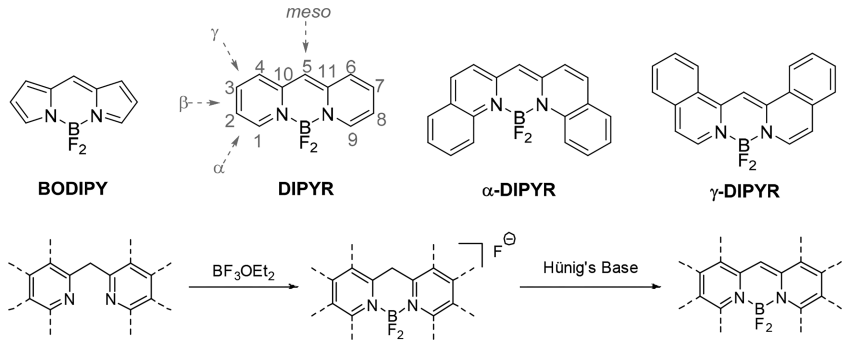

Figure 1. Structures, from left to right, of BODIPY, DIPYR, α-DIPYR, and γ-DIPYR are depicted. The *meso* position is labeled according to convention. The synthetic scheme used to prepare the three DIPYR dyes is shown below.

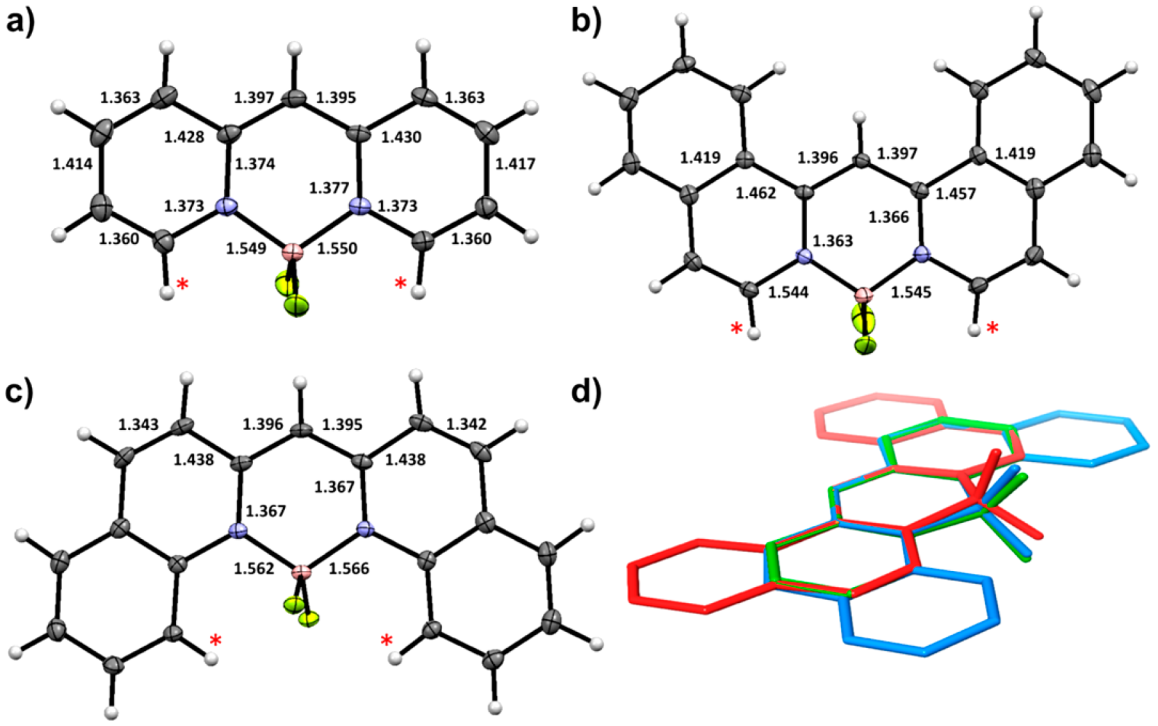

Figure 2. Molecular structures of DIPYR (a), γ-DIPYR (b), and α-DIPYR (c) are presented with labeled bond lengths. Carbon (gray), nitrogen (blue), boron (pink), and fluorine (yellow) residues are depicted as thermal ellipsoids at 50% probability; hydrogen atoms (light gray) are drawn as spheres with a radius of 0.15 Å. The central rings of each of the three dyes DIPYR (green), α-DIPYR (blue), and γ-DIPYR (red) are overlaid in part d to show the subtle variation in central-ring puckering of the BF_2 moiety.

our interest in the study of the parent DIPYR dyes with methine at the *meso* position. Herein, we report the synthesis and structural and photophysical properties of this promising new family of pyridine-, quinoline-, and isoquinoline-derived fluorescent dyes. We find that benzannulation of DIPYR leads to higher absorptivity and substantial increases in luminescent efficiency, with quantum yields (Φ_{PL} = 0.8) that approach values comparable to those of the most highly efficient BODIPY dyes. The increase in fluorescent efficiency in the quinoline and isoquinoline DIPYR derivatives is attributed to a decrease in the rate of intersystem crossing caused by a change in energetic ordering of the S_1 and T_2 excited states.

RESULTS AND DISCUSSION

The methylene-bridged heteroaryl precursors to DIPYR dyes were prepared according to literature procedures.[20,21] The synthetic route to DIPYR dyes (Figure 1) involves first borylating the diheteroarylmethane ligand by refluxing in the presence of boron trifluoride diethyl etherate, to prepare a fluoride salt which precipitates from the reaction mixture upon cooling. The salt is then deprotonated with an excess of Hünig's base to produce the final product in 38% yield. This method is similar to one used to obtain *meso*-cyano DIPYRs,[19] and was also used to prepare α-DIPYR and γ-DIPYR in 39% and 36% yields, respectively. It is interesting to note that, in the case of dipyridylamine ligands, the deprotonation step occurs without the need for the addition of base. The early report,[18] comparing DIPYR (methane-bridged) with dipyridylamine (nitrogen-bridged) analogues, did not include a deprotonation step, and thus isolation of the intermediate salt *in lieu* of DIPYR itself may be the source of confusion in the literature regarding the emissive properties of DIPYR dyes.

Molecular structures of DIPYR, γ-DIPYR, and α-DIPYR obtained by X-ray diffraction analysis are shown in Figure 2 (crystal packing figures are available in the SI). The carbon–carbon bonds of DIPYR mimic a pattern of alternating short

DOI: 10.1021/acs.joc.7b00786
J. Org. Chem. 2017, 82, 7215–7222

(C1−C2 and C3−C4) and long (C2−C3 and C4−C5) distances similar to those found in the aromatic rings of anthracene.[22] An intermediate distance to the *meso*-carbon (C5−C6) is also found for the related C−C bond in anthracene. The carbon−nitrogen bond distances (C1−N1 and C5−N1) are elongated relative to the values found in pyridine (C−N = 1.337 Å) and more closely correspond to the elongated C−C bond lengths for the equivalent atom positions in anthracene. This bond-length alternation pattern is preserved in the benzannulated derivatives, although the distances between the bridging C−C atoms are lengthened relative to those of the parent structure. A narrow range for the boron−nitrogen (1.544−1.566 Å) and boron−fluorine (1.390−1.404 Å) bond lengths in all three derivatives indicates closely related bonding interactions between these atoms. Interestingly, in all three compounds the central six-membered borocyclic ring adopts a boatlike conformation, wherein the BF_2 moiety and *meso*-carbon lie above the plane of the central ring, with the BF_2 group residing further out-of-plane (Figure 2d). The distance to which the BF_2 moiety is out-of-plane (d_{op}) is larger in γ-DIPYR (d_{op} = 0.23 Å) than in either DIPYR (d_{op} = 0.09 Å) or α-DIPYR (d_{op} = 0.04 Å). Although γ-DIPYR exhibits a larger distortion relative to the other two DIPYRs, the small deviation from planarity in the borocyclic ring may simply be a result of crystal packing forces.

It is useful to compare the structural characteristics of the DIPYR dyes to those of analogous BODIPY dyes. The variation in C−C bond lengths in the five-membered ring of BODIPY is smaller (1.370−1.410 Å)[14] than in DIPYR (1.360−1.430 Å), suggesting a greater degree of cyanine-like interaction between the canonical resonance structures of BODIPY than that of DIPYR. Bond distances between B−N and B−F are comparable in both types of chromophores, and both exhibit slight puckering of the boron atom out of the plane of the borocyclic ring (d_{op} = 0.146 Å in BODIPY and 0.09 Å in DIPYR). One significant difference between BODIPY and the DIPYR derivatives is the average distance between the fluorine atoms and the nearest hydrogen atoms (Figure 2, starred, for DIPYRs). The closest intramolecular H···F distances in the parent BODIPY (3.0 Å) fall outside the Van der Waals radii of the two atoms (2.67 Å).[23] In contrast, the equivalent protons in DIPYRs are positioned much closer to the fluorine atoms; the shortest intramolecular H···F distances found in DIPYR and γ-DIPYR are 2.55 and 2.43 Å, respectively, whereas the benzannulated rings of α-DIPYR place the atoms in even closer proximity (H···F = 2.34−2.49 Å). The effect of the short H···F distances is manifested in the coupling of the ^{1}H NMR resonances at these positions. The doublets in DIPYR (δ = 7.90 ppm, $^3J_{HH}$ = 5.5 Hz) and γ-DIPYR (δ = 7.88 ppm, $^3J_{HH}$ = 7.0 Hz) are broadened because of through-space coupling to the ^{19}F atoms,[24] and the corresponding protons in α-DIPYR (δ = 8.57 ppm) are clearly resolved into a doublet of triplets ($^3J_{HH}$ = 8.8 Hz, $^4J_{FH}$ = 3.5 Hz).

The electrochemical properties of the dyes were examined using cyclic voltammetry (Figures S3−S5); redox potentials versus an internal ferrocene standard are given in Table 1. The oxidation waves in all three materials are irreversible. The reduction wave in DIPYR is quasireversible, while waves in both α-DIPYR and γ-DIPYR are reversible. The irreversible oxidation in DIPYR dyes may be the result of the coupling of two oxidized molecules, a phenomenon which has been observed during the oxidation of BODIPYs and cyanines.[25−28]

Oxidation of DIPYR occurs at a much lower potential (E_{ox} = 0.14 V) than in BODIPY (E_{ox} = 1.35 V),[29] whereas the reduction potential is correspondingly more negative (DIPYR, E_{red} = −2.32 V; BODIPY, E_{red} = −1.05 V).[28,30] The redox potentials of both α-DIPYR and γ-DIPYR are anodically shifted relative to the parent compound indicating stabilization of both frontier MOs upon benzannulation, with the LUMO stabilized to a greater degree than the HOMO.

Table 1. Redox Potentials (V vs Fc^+/Fc)[a]

	E_{ox}	E_{red}	ΔE_{redox}
DIPYR	0.14	−2.32	2.48
α-DIPYR	0.40	−1.95	2.35
γ-DIPYR	0.27	−2.07	2.34

[a]In acetonitrile with 0.1 M TBAF.

The photophysical properties of the dyes were characterized using UV−vis absorption and emission spectroscopies (Figure 3); data are summarized in Table 2. All of the DIPYRs display

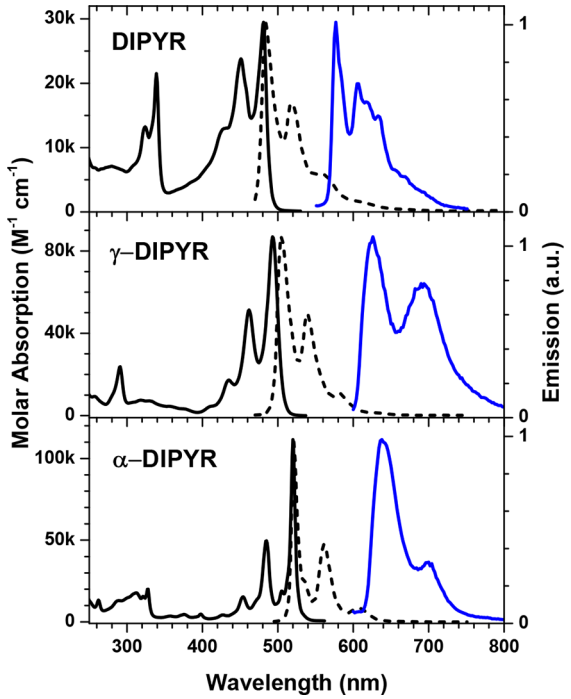

Figure 3. Absorption (—) and normalized (– – –) fluorescence and phosphorescence (blue) spectra recorded in methylcyclohexane; left axis is molar absorbance, right axis is normalized emission intensity.

intense ($\varepsilon > 10^4$ M^{-1} cm^{-1}), vibronically structured absorption bands in the UV−vis spectrum. The line shape of the DIPYR absorbance band is similar to the profile reported for *meso*-cyano DIPYR.[19] The lowest energy absorption bands become more intense and red-shift in the benzannulated derivatives. The vibronic manifolds display major progressions of 1475 cm^{-1}, similar to the spacings found in anthracene, and the 0−0 transitions become stronger and more intense than the 0−1 transitions in the benzannulated derivatives. The lowest absorption transitions in all derivatives display small hypsochromic shifts (<10 nm) going from nonpolar (methylcyclohexane) to polar (acetonitrile) solutions.

Interestingly, the absorption line shape of DIPYR is solvent-dependent; the 0−1 peak of the vibronic progression gradually increases in intensity with increasing solvent polarity, becoming more intense than the 0−0 transition in acetonitrile solution

DOI: 10.1021/acs.joc.7b00786
J. Org. Chem. 2017, 82, 7215−7222

Table 2. Photophysical Properties of DIPYR Dyes[a]

	absorption λ_{max} (nm)	ε (M^{-1} cm^{-1})	emission λ_{max} (nm)	Φ_{PL}	τ (ns)	k_r (10^8 s^{-1})	k_{nr} (10^8 s^{-1})
DIPYR	481 (476)	2.9×10^4	484 (496) 482[b], 577[c]	0.17 (0.085)	1.9 (1.6) 2.0[b]	0.91 (0.53)	4.5 (5.7)
α-DIPYR	520 (515)	1.1×10^5	520 (521) 520[b], 638[c]	0.77 (0.77)	5.7 (5.0) 4.7[b]	1.4 (1.5)	0.41 (0.46)
γ-DIPYR	500 (493)	8.7×10^4	504 (504) 504[b], 626[c]	0.80 (0.75)	3.9 (4.1) 3.6[b]	2.0 (1.8)	0.51 (0.61)

[a]Measurements acquired at room temperature in methylcyclohexane (acetonitrile). [b]Fluorescence at 77 K in methylcyclohexane. [c]Phosphorescence at 77 K in methylcyclohexane.

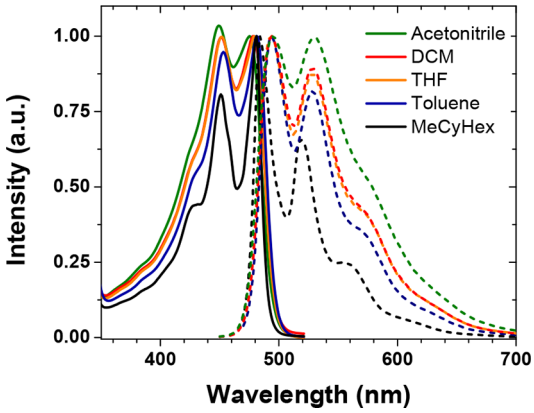

Figure 4. Normalized absorption (—) and emission (– – –) spectra of DIPYR in solvents of increasing polarity. It is noted that the relative intensity of the 0–1 vibronic feature increases with increasing polarity, suggesting the presence of a second, underlying absorptive feature which is solvent-dependent.

(Figure 4). In contrast, aside from an increase in the inhomogeneous broadening in acetonitrile, the absorption line shapes for α-DIPYR and γ-DIPYR are similar in both solvents. The change in the line shape with solvent polarity for DIPYR suggests the presence of a second, weaker transition lying at a slightly higher energy than the S_0–S_1 transition. This supposition is supported by theoretical calculations of the excited state (*vida infra*). Another notable feature in the absorption spectra is an extremely narrow line width for the 0–0 transition of α-DIPYR, which has a full width half-maximum (fwhm) of 250 cm^{-1}. This transition is much narrower than the 0–0 transition in γ-DIPYR (fwhm = 700 cm^{-1}) and even less than the value found for the corresponding feature of anthracene (fwhm = 440 cm^{-1}). The narrow line width for the 0–0 transition, along with the large ratio between the 0–0 and 0–1 transitions, indicates that there is minimal structural distortion in the excited state of α-DIPYR.

All of the DIPYR derivatives are highly luminescent in solution and display small Stokes shifts (<5 nm) in nonpolar solvents. A noticeable asymmetry is present in the mirror-image relationship between absorption and emission in DIPYR, consistent with the absorption profile being distorted by an S_2 state lying at slightly higher energy than the S_1 state. In contrast, the absorption and emission spectra of the benzannulated derivatives display a near-perfect mirror symmetry. DIPYR has a photoluminescent quantum yield (Φ_{PL}) of 17% in methylcyclohexane and 8.5% in acetonitrile, whereas the values for α- and γ-DIPYR are much higher (Φ_{PL} = 77% and 80%, respectively) and nearly solvent-independent. The radiative rate constants (k_r's) are similar in value among all three derivatives ($k_r = 0.91–2.0 \times 10^8$ s^{-1}), whereas the rate for nonradiative decay (k_{nr}) of DIPYR in methylcyclohexane ($k_{nr} = 4.5 \times 10^8$ s^{-1}) is nearly an order of magnitude larger than values for α- and γ-DIPYR ($k_{nr} \approx 4.5 \times 10^7$ s^{-1}). The notably faster rate for nonradiative decay in DIPYR is not the result of structural distortions in the excited state as no major change in the luminescent lifetime (τ) values occurs in either fluid solution at room temperature (τ = 1.9 ns) or rigid media at 77 K (τ = 2.0 ns). A more plausible explanation for the large k_{nr} value of DIPYR is a fast rate for intersystem crossing (ISC) between singlet and triplet states. Support for this mechanistic hypothesis is based on the fact that phosphorescent emission (E_{0-0} = 577 nm) is readily observed in the parent DIPYR in frozen methylcyclohexane at 77 K, whereas none is observed under similar conditions for α- and γ-DIPYR. It is possible, however, to record phosphorescence from the benzannulated compounds in frozen solutions using more rigorous conditions of gated detection, along with the addition of iodomethane to promote ISC through an external heavy atom effect (Figure 3).

The electronic characteristics of DIPYR dyes in the gas phase were examined using both time-dependent density functional (TD-DFT) and extended multiconfigurational quasidegenerate second-order perturbation (XMCQDPT2)[31] theoretical calculations (see the SI for a thorough analysis of computational methods). The XMCQDPT2 calculations were employed on account of recent studies where it has been determined that optical transitions in *meso*-cyano DIPYR and related cyanine-type dyes are multireference in nature and are accompanied by a significant double excitation character in their excited states.[32] Singlet excitation energies calculated for these pseudoaromatic dyes using single-reference methods such as TD-DFT are found to have errors greater than 0.3 eV.[32,33] However, despite the large absolute errors, the calculated TD-DFT values for this class of molecules can be scaled linearly with experimental excitation energies.[33]

The DFT calculations replicate the pattern of C–C and C–N bond length alternation found in the X-ray structures of the molecules, including an out-of-plane distortion (d_{op} = 0.42 Å) of the BF_2 group in the six-membered borocyclic ring in DIPYR, but showed none of these patterns for either α- or γ-DIPYR. In contrast, the geometry calculated for the excited S_1 state does show an out-of-plane distortion in γ-DIPYR (d_{op} = 0.32 Å), as well as in DIPYR (d_{op} = 0.50 Å), but virtually none for α-DIPYR (d_{op} = 0.001 Å). Out-of-plane distortion of the BF_2 moiety in the α-DIPYR is likely impeded by H···F steric conflicts between the nearby protons of the benzannulated ring and the fluorine atoms that lie above and below the molecular plane, as made evident by through-space coupling of ^1H to ^{19}F in the NMR studies discussed previously. The separation between these atoms is calculated to be 2.36 Å, which places them 0.4 Å closer than the sum of their Van der Waals radii. Moreover, energies calculated for out-of-plane vibrations of the boron atom and flanking aromatic rings range between 70 and 225 cm^{-1}, similar to values found in BODIPY.[34] Therefore, the extremely narrow line width for the 0–0 transition of α-DIPYR in methylcyclohexane is likely due to the inhibition of out-of-plane vibronic motions of the BF_2 group.

DOI: 10.1021/acs.joc.7b00786
J. Org. Chem. 2017, 82, 7215–7222

The nodal characteristics for the frontier orbitals of DIPYR are compared here with those of BODIPY as they share distinct similarities and differences (Figure 5). In an idealized planar

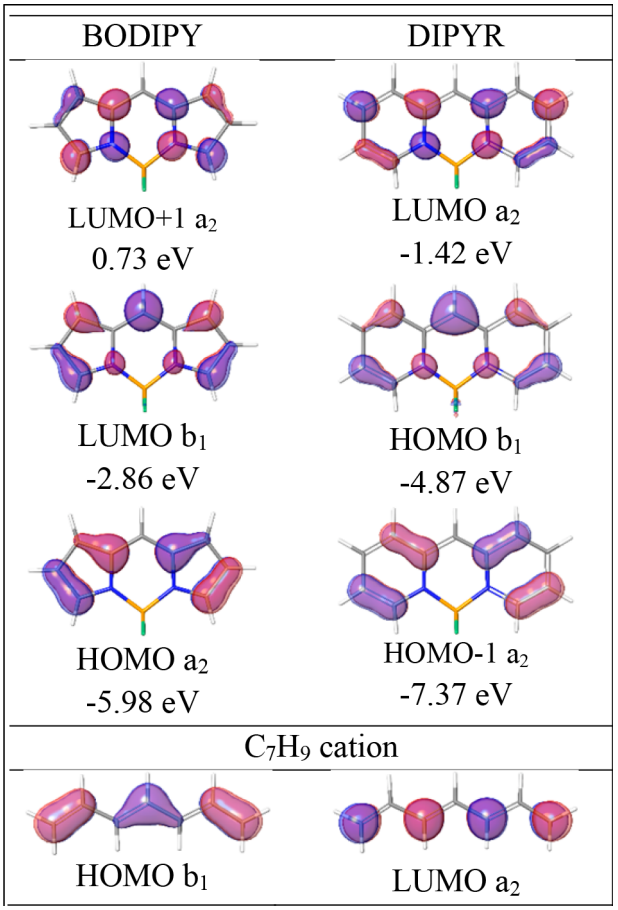

Figure 5. Orbital contributions to the frontier molecular orbitals in BODIPY dyes (left) compared with those in DIPYR dyes (right).

BODIPY (C_{2v} point group), the HOMO and LUMO + 1 have a_2 symmetry whereas the LUMO is b_1. Hence, both the HOMO and LUMO + 1 have a node that lies on the C_2 axis of the molecule, whereas the LUMO has a substantial atomic orbital density at the *meso* carbon atom. The same symmetric configuration appears in DIPYR; however, the exchange of pyridyl for pyrrole moieties shifts the orbital relationship, such that the HOMO − 1 and LUMO now have b_1 symmetry and the HOMO has a_2. This change in electronic structure leads to a large atomic orbital contribution localized at the *meso* position of the HOMO in DIPYR. However, despite these differences in orbital-symmetry labels, the HOMO−LUMO transition dipole moment in both molecules is polarized along the long axis of the molecule, perpendicular to the permanent dipole oriented along the short (C_2) axis. It is this orthogonal arrangement of (long) transition and (short) permanent dipole moments that leads to a high molar absorptivity that is relatively insensitive to solvent polarity in both molecules.[35]

In addition, it is worth noting that the nodal characteristics of the top half of DIPYR are identical to those of the C_7H_9 cation. This orbital pattern, where nodes bisect every other carbon atom in the HOMO and LUMO, is a feature common to nonalternant hydrocarbons and leads to intense, narrow absorption bands in chromophores such as cyanine dyes.[36]

The relative energies calculated for the valence orbitals are in good agreement with the electrochemical oxidation and reduction potentials. The calculated energies for the HOMO and LUMO in DIPYR are destabilized by approximately 1.1 and 1.3 eV, respectively, compared to the energies for the corresponding orbitals in BODIPY. Likewise, HOMO and LUMO energies calculated for α- and γ-DIPYR reflect the relative stabilization of these orbitals determined from their corresponding redox potentials (for α-DIPYR, HOMO = −5.00 eV, LUMO = −1.96 eV; for γ-DIPYR, HOMO = −5.01 eV, LUMO = −1.91 eV). Although extension of the π-system in chromophores by benzannulation is typically understood to induce a bathochromic shift of the absorption and emission bands, the location of benzannulation plays a key role in modulating this effect (Hanson's rules).[37] Compared to that for DIPYR, the decrease in the HOMO−LUMO energy gap for α- and γ-DIPYR (0.31 and 0.35 eV, respectively) corresponds to the respective red-shifts of 0.20 eV (34 nm) and 0.10 eV (19 nm) in their E_{0-0} energies for the S_1 state.

The relative energies of the S_1 and S_2, and T_1 and T_2 states (Table 3) were calculated for each of the three DIPYR derivatives and evaluated to shed light on the effect of benzannulation in this family of dyes. Both S_0−S_1 and S_0−T_1 transitions are primarily between the HOMO and LUMO, polarized along the long molecular axis, whereas the S_0−S_2 and S_0−T_2 transitions are predominantly between the HOMO and LUMO + 1, polarized along the short axis of the molecules such that they lie anti-parallel to the molecular dipole. Consequently, we can predict that the S_0−S_2 and S_0−T_2 transitions will be destabilized in polar environments. After comparison with experiment results, a −0.44 eV shift in energy was applied to all calculated singlet energies for this family of DIPYR dyes. This seemingly arbitrary correction factor is consistent with the large but linear difference between state energies derived using TD-DFT versus experimental values in BODIPYs, cyanines, and other similar pseudoaromatic dyes.[32,33] The discrepancy between experimental and theoretical energies in this case stems from a failure of TD-DFT methods to account for the double excitation character of singlet states in these systems.[32] The correction factor was

Table 3. Calculated (DFT: B3LYP/6-31G) and Experimental State Energies in DIPYR Dyes in nm (eV)**

	S_2 calcd[a]	S_1 calcd[a]	S_1 expt	T_2 calcd	T_1 calcd	T_1 expt
DIPYR	451 (2.75)	461 (2.69)	482 (2.57)	511 (2.43)	587 (2.11)	577 (2.15)
	f = 0.029	f = 0.232				
α-DIPYR	444 (2.79)	533 (2.33)	524 (2.37)	480 (2.58)	668 (1.86)	638 (1.94)
	f = 0.030	f = 0.463				
γ-DIPYR	415 (2.99)	515 (2.41)	504 (2.46)	450 (2.76)	658 (1.89)	626 (1.98)
	f = 0.030	f = 0.590				

[a]Calculated singlet energies were corrected by subtracting 0.44 eV from the computational output.

DOI: 10.1021/acs.joc.7b00786
J. Org. Chem. 2017, 82, 7215−7222

determined by the mean difference between calculated and experimentally observed singlet state energies (S_1, S_2, and S_3) across the series. However, the calculated triplet state energies are in relatively good agreement, i.e., <100 mV difference between the calculated and experimental values, as XMCQDPT2 calculations show that both triplet states T_1 and T_2 can be accurately described within the TD-DFT framework because of minimal (<1.2%) contribution from double excitations (see the SI for calculation results).

With the calculated singlet state energies in hand, it is possible to explain the observed absorption and emission spectral characteristics for the DIPYR chromophore. DIPYR displays three strong absorption bands in the UV−vis spectrum, corresponding to transitions from the S_0 ground state to the S_1, S_2, and S_3 states. The S_1 and S_2 states in DIPYR are close enough in energy to have overlapping transition manifolds, with oscillator strength (f) of the S_0−S_1 transition being roughly an order of magnitude larger than that of the S_0−S_2 transition. Thus, the vibronic progression of the S_0−S_1 absorption band is distorted by the underlying S_0−S_2 transition. The S_0−S_2 transition dipole moment is polarized along the short axis of the dye, parallel to the molecular dipole. Therefore, the energy of the S_2 state is expected to be strongly affected in polar media, thereby shifting the wavelength of the S_0−S_2 transition. In contrast, the S_0−S_1 transition dipole moment lies along the long axis of the molecule, and as such displays a weak hypsochromic dependence on solvent polarity. The close juxtaposition in energy between the S_1 and S_2 states induces a polarity-dependent relationship in the line shape of the lowest energy absorption bands in solution, as the S_0−S_2 transition will shift in energy with increasing polarity whereas the S_0−S_1 transition will remain relatively unchanged (Figure 4). Consequently, the S_0−S_2 transition will be mixed into the lowest excited state to a greater extent in polar media, as made evident by the relative increase in the 0−1 vibronic feature in the absorption spectrum of DIPYR in polar solvents. This competition between transitions is reflected in the radiative rate constants of DIPYR in methylcyclohexane ($k_r = 9.1 \times 10^7$ s^{-1}) versus that in acetonitrile ($k_r = 5.3 \times 10^7$ s^{-1}), where the stabilizing effect of the polar solvent increases the contribution from the weaker, dipole-containing S_2 state. In the case of both α- and γ-DIPYR, the S_0−S_2 transition does not overlap with the S_0−S_1 transition, and thus the line shape of the latter absorption band and radiative rate constants displayed are unchanged upon an increase in solvent polarity.

Another important change brought about by benzannulation is a relative reordering of the S_1 and T_2 state energies. The energy of the T_2 state in DIPYR is calculated to be lower than that of the experimental S_1 state, whereas the energies of the T_2 states calculated for α- and γ-DIPYR are greater than those of the experimental S_1 states (see Figure 6). This difference in ordering between the S_1 and T_2 state energies is due to a stabilization of the LUMO upon benzannulation (ca. −0.50 eV) while the LUMO + 1 remains mostly unchanged (−0.15 eV in α-DIPYR and +0.08 eV in γ-DIPYR). The relative ordering of state energies in DIPYR is what leads to the low Φ_{PL} that is further suppressed by an increase in solvent polarity, since ISC from S_1 to T_2 is symmetry-allowed and favored by the close proximity in energy between the two states.[38] The net result in DIPYR is a fast rate for ISC ($k_{ISC} > 10^9$ s^{-1}) that outcompetes radiative decay from the S_1 state. This energetic situation ($T_2 < S_1$) is similar to that present in anthracene and considered responsible for its high rate of intersystem crossing and

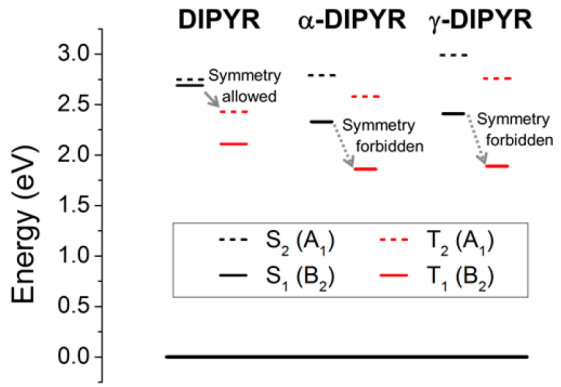

Figure 6. Intersystem crossing from S_1 to T_2 occurs rapidly in DIPYR, as the process is both exergonic and symmetry-allowed. In α- and γ-DIPYR, however, the only exergonic ISC mechanism is symmetry-forbidden, and thus occurs too slowly to compete with fluorescence.

consequent luminescent efficiency ($k_{ISC} = 10^8$ s^{-1}, $\Phi_{PL} = 0.24$).[39] In contrast, the higher energy of the T_2 states compared to that of the S_1 states in α- and γ-DIPYR makes ISC to T_2 an endothermic, unfavorable process. Therefore, the only pathway for ISC is directly from S_1 to T_1, which is symmetry-forbidden, and thus a slow process ($k_{ISC} < 10^9$ s^{-1}) that results in high Φ_{PL} independent of solvent polarity. Support for this hypothesis is provided by phosphorescence emission experiments. Phosphorescence from DIPYR is readily observed in frozen methyl cyclohexane, whereas more rigorous methods of gated detection and treatment with a heavy atom are needed to observe phosphorescence emission in the benzannulated derivatives, consistent with slow ISC and thus a low yield of T_1 for the latter compounds.

CONCLUSION

In summary, a small family of simple pyridine-, quinoline-, and isoquinoline-based fluorophores, termed DIPYR dyes, has been characterized and described. The reason for the relatively low Φ_{PL} in the DIPYR parent is the energetic alignment of the T_2 state just below the S_1 state, which leads to relatively efficient intersystem crossing that is competitive with fluorescence, followed by nonradiative decay from the triplet. Benzannulation of the DIPYR moves the T_2 state higher in energy than the S_1 state, thereby leading to a significant decrease in the rate of intersystem crossing and a significant increase in the fluorescent quantum efficiency. The coupling of broad spectral width and high absorption coefficients is promising for generating large carrier densities in organic photovoltaics. Significant opportunity remains for additional manipulation of this library of dyes, in which alkylation, aza and push−pull substitution, and π-extension are each expected to be useful methods for the modulation of absorption and emission onsets and intensities; a keen understanding of the molecular orbital characteristics of these compounds will play a major role in color- and intensity-tuning the absorption and emission profiles of new derivatives. We expect that an expanded library of these dyes will serve as a useful tool for fluorescent labeling applications. Further investigation into this class of dyes and their applications to light harvesting and energy conversion are actively underway.

EXPERIMENTAL SECTION

Instrumentation. UV−vis spectra were recorded on a Hewlett-Packard 4853 diode array spectrometer. Photoluminescence spectra

DOI: 10.1021/acs.joc.7b00786
J. Org. Chem. 2017, 82, 7215−7222

were measured using a QuantaMaster Photon Technology International phosphorescence/fluorescence spectrofluorometer. Quantum yield measurements were carried out using a Hamamatsu C9920 system equipped with a xenon lamp, calibrated integrating sphere, and model C10027 photonic multichannel analyzer (PMA). Photoluminescence lifetimes were measured by time-correlated single-photon counting using an IBH Fluorocube instrument equipped with an LED excitation source. Molar extinction coefficients were obtained by plotting solutions at four concentrations between 0.1 and 0.9 on a Beer's Law plot, with y intercept set to zero. Line fitting for all samples provided R^2 values greater than 0.98. Excitation, emission, photoluminescence quantum yield, and lifetime measurements were acquired from solutions at maximum optical densities between 0.1 and 0.2 to minimize the effects of solute−solute interactions. Room-temperature photophysical measurements were recorded in methylcyclohexane or acetonitrile, and cryogenic photophysical measurements were carried out in methylcyclohexane at 77 K. Methyl iodide was added to α-DIPYR and γ-DIPYR to enhance the rate of ISC in order to observe a phosphorescence emission. Reported phosphorescence spectra were acquired in methylcyclohexane at 77 K using a gated emission scan with 30 μs delay. NMR spectra were recorded on a Varian 400 NMR spectrometer and referenced to the residual proton resonance of chloroform ($CDCl_3$) solvent at 7.26 ppm. Matrix-assisted laser desorption/ionization (MALDI) mass spectroscopy data was acquired on a Bruker Autoflex Speed LRF.

Computational Methods. All calculations were performed using the Jaguar 8.4 (release 12) software package on the Schrodinger Material Science Suite (v2016-2). Gas-phase geometry optimizations were calculated using the CAM-B3LYP functional with the 6-31G** basis set as implemented in Jaguar. We also employed the extended multiconfigurational quasidegenerate second-order perturbation theory[40] (XMCQDPT2) method implemented in the Firefly quantum chemistry package[41] to incorporate dynamic correlation to the CASSCF calculations.

General Synthesis. All reagents were purchased from Sigma-Aldrich and used without purification. Anhydrous 1,2-dichloroethane was purchased from EMD Millipore.

A 15 mM solution of diheteroarylmethane ligand in dry 1,2-dichloroethane was prepared in a N_2-purged Schlenk flask equipped with a magnetic stir bar and fitted with a reflux condenser. The flask was submerged in a preheated oil bath and brought to reflux, at which time 2.0 equiv of boron trifluoride diethyl etherate was added dropwise, causing the color to change from deep yellow to an opaque, pale yellow, corresponding to the rapid formation of precipitate. The solution was stirred for 2 h at reflux, then cooled to room temperature, and treated with 5 equiv *N*,*N*-diisopropylethylamine, causing the precipitate to dissolve and the solution to turn deep yellow-orange with a bright green fluorescence. The solution was washed with water, and the aqueous layer was separated and extracted 3 times with dichloromethane. The organic layers were combined, dried over sodium sulfate, filtered, and reduced to a bright orange polycrystalline solid by rotary evaporation. The products were purified by silica-gel flash chromatography with the eluent 30% dichloromethane in hexanes, followed by recrystallization. Single-crystal X-ray quality crystals were obtained for DIPYR and γ-DIPYR by recrystallization from the slow diffusion of hexanes into a concentrated dichloromethane solution. Single crystals of α-DIPYR were obtained by very slow cooling (in a Dewar) of a concentrated hot methanol solution to −48 °C for 72 h.

The synthesis of DIPYR yielded 2.54 g (38%), as orange crystals with green reflectance. ^{1}H NMR (400 MHz, $CDCl_3$) δ 7.94−7.86 (br d, 2H, J = 5.5 Hz), 7.25 (ddd, J = 8.9, 6.7, 1.6, 2H), 6.82 (d, J = 8.8 Hz, 2H), 6.50 (dd, J = 6.7, 1.2 Hz, 2H), 5.36 (s, 1H). ^{13}C{^{1}H} NMR (101 MHz, $CDCl_3$) δ 149.3, 136.8, 135.6, 121.2, 111.4, 111.4, 85.3. Spectra match those reported in the literature.[17] MS (MALDI) m/z calcd for $C_{11}H_9BF_2N_2^+$ 218.083 $[M]^+$; found 217.906.

The synthesis of α-DIPYR yielded 0.27 g (39%), as orange crystals with green reflectance. ^{1}H NMR (400 MHz, $CDCl_3$) δ 8.57 (dt, J = 8.8, 3.5 Hz, 2H), 7.64−7.54 (m, 4H), 7.51 (dd, J = 7.8, 1.5 Hz, 2H), 7.32−7.26 (m, 2H), 6.85 (d, J = 9.0 Hz, 2H), 5.48 (s, 1H). ^{13}C{^{1}H} NMR (101 MHz, $CDCl_3$) δ 149.7, 139.8, 136.5, 130.8, 128.1, 124.8, 123.8, 121.9, 121.4 (t, J = 8.3 Hz), 91.5. Anal. Calcd for $C_{19}H_{13}BF_2N_2$: C, 71.73; H, 4.12; N, 8.81. Found: C, 71.35; H, 4.24; N, 8.55. A melting temperature determination was attempted, but sublimation was observed at atmospheric pressure in the capillary tube at 217 °C. MS (MALDI) m/z calcd for $C_{19}H_{13}BF_2N_2^+$ 318.114 $[M]^+$; found 317.999.

The synthesis of γ-DIPYR yielded 0.84 g (36%), as red-orange crystals with green reflectance. ^{1}H NMR (400 MHz, $CDCl_3$) δ 8.37 (d, J = 7.8 Hz, 2H), 7.91−7.85 (br d, J = 7.0 Hz, 2H), 7.68 (ddd, J = 8.0, 6.8, 1.2 Hz, 2H), 7.64−7.56 (m, 4H), 7.16 (s, 1H), 6.97−6.92 (br d, J = 7.1 Hz, 2H). ^{13}C{^{1}H} NMR (101 MHz, $CDCl_3$) δ 148.6, 135.1, 131.7, 130.9, 127.6, 127.0, 124.9, 124.7, 112.1, 81.4. Anal. Calcd for $C_{19}H_{13}BF_2N_2$: C, 71.73; H, 4.12; N, 8.81. Found: C, 71.57; H, 4.16; N, 8.57. A melting temperature determination was attempted, but sublimation was observed at atmospheric pressure in the capillary tube at 258 °C. MS (MALDI) m/z calcd for $C_{19}H_{13}BF_2N_2^+$ 318.114 $[M]^+$; found 318.010.

■ ASSOCIATED CONTENT

Supporting Information

The Supporting Information is available free of charge on the ACS Publications website at DOI: 10.1021/acs.joc.7b00786.

Full NMR spectra, cyclic voltammograms, TD-DFT data and figures, ligand synthesis, absorption and emission spectra (PDF)

Crystallographic data for DIPYR (CIF)

Crystallographic data for α-DIPYR (CIF)

Crystallographic data for γ-DIPYR (CIF)

■ AUTHOR INFORMATION

Corresponding Author

*E-mail: met@usc.edu.

ORCID

Mark E. Thompson: 0000-0002-7764-4096

Notes

The authors declare no competing financial interest.

■ ACKNOWLEDGMENTS

Financial support from the Office of Basic Energy Sciences at the Department of Energy (DE-SC0016450) is gratefully acknowledged. We thank Dr. Ralf Haiges for help in refining the crystal structures.

■ REFERENCES

(1) Kurata, S.; Kanagawa, T.; Yamada, K.; Torimura, M.; Yokomaku, T.; Kamagata, Y.; Kurane, R. *Nucleic Acids Res.* **2001**, *29*, 34e.

(2) Li, X.; Traganos, F.; Melamed, M. R.; Darzynkiewicz, Z. *Cytometry* **1995**, *20*, 172−180.

(3) Meng, Q.; Kim, D. H.; Bai, X.; Bi, L.; Turro, N. J.; Ju, J. *J. Org. Chem.* **2006**, *71*, 3248−3252.

(4) Metzker, M. L.; Lu, J.; Gibbs, R. A. *Science* **1996**, *271*, 1420−1422.

(5) Karolin, J.; Johansson, L. B. A.; Strandberg, L.; Ny, T. *J. Am. Chem. Soc.* **1994**, *116*, 7801−7806.

(6) Sunahara, H.; Urano, Y.; Kojima, H.; Nagano, T. *J. Am. Chem. Soc.* **2007**, *129*, 5597−5604.

(7) Baruah, M.; Qin, W.; Basarić, N.; De Borggraeve, W. M.; Boens, N. *J. Org. Chem.* **2005**, *70*, 4152−4157.

(8) Qi, X.; Jun, E. J.; Xu, L.; Kim, S.-J.; Joong Hong, J. S.; Yoon, Y. J.; Yoon, J. *J. Org. Chem.* **2006**, *71*, 2881−2884.

(9) Zhang, D.; Martin, V.; Garcia-Moreno, I.; Costela, A.; Perez-Ojeda, M. E.; Xiao, Y. *Phys. Chem. Chem. Phys.* **2011**, *13*, 13026−13033.

DOI: 10.1021/acs.joc.7b00786
J. Org. Chem. 2017, 82, 7215−7222

(10) Chen, J. J.; Conron, S. M.; Erwin, P.; Dimitriou, M.; McAlahney, K.; Thompson, M. E. *ACS Appl. Mater. Interfaces* **2015**, *7*, 662−669.
(11) Erten-Ela, S.; Yilmaz, M. D.; Icli, B.; Dede, Y.; Icli, S.; Akkaya, E. U. *Org. Lett.* **2008**, *10*, 3299−3302.
(12) Hendrickson, H. S.; Hendrickson, E. K.; Johnson, I. D.; Farber, S. A. *Anal. Biochem.* **1999**, *276*, 27−35.
(13) Loudet, A.; Burgess, K. *Chem. Rev.* **2007**, *107*, 4891−4932.
(14) Arroyo, I. J.; Hu, R.; Merino, G.; Tang, B. Z.; Peña-Cabrera, E. *J. Org. Chem.* **2009**, *74*, 5719−5722.
(15) Schmitt, A.; Hinkeldey, B.; Wild, M.; Jung, G. *J. Fluoresc.* **2009**, *19*, 755−758.
(16) Tram, K.; Yan, H.; Jenkins, H. A.; Vassiliev, S.; Bruce, D. *Dyes Pigm.* **2009**, *82*, 392−395.
(17) Douglass, J. E.; Barelski, P. M.; Blankenship, R. M. *J. Heterocycl. Chem.* **1973**, *10*, 255−257.
(18) Sathyamoorthi, G.; Soong, M.-L.; Ross, T. W.; Boyer, J. H. *Heteroat. Chem.* **1993**, *4*, 603−608.
(19) Kubota, Y.; Tsuzuki, T.; Funabiki, K.; Ebihara, M.; Matsui, M. *Org. Lett.* **2010**, *12*, 4010−4013.
(20) Dyker, G.; Muth, O. *Eur. J. Org. Chem.* **2004**, *2004*, 4319−4322.
(21) Stephens, D. E.; Nguyen, V. T.; Chhetri, B.; Clark, E. R.; Arman, H. D.; Larionov, O. V. *Org. Lett.* **2016**, *18*, 5808−5811.
(22) Cruickshank, D. W. J.; Sparks, R. A. *Proc. R. Soc. London, Ser. A* **1960**, *258*, 270.
(23) Bondi, A. *J. Phys. Chem.* **1964**, *68*, 441−451.
(24) Hierso, J. C. *Chem. Rev.* **2014**, *114*, 4838−4867.
(25) Parton, R. L.; Lenhard, J. R. *J. Org. Chem.* **1990**, *55*, 49−57.
(26) Lenhard, J. R.; Parton, R. L. *J. Am. Chem. Soc.* **1987**, *109*, 5808−5813.
(27) Lenhard, J. R.; Cameron, A. D. *J. Phys. Chem.* **1993**, *97*, 4916−4925.
(28) Nepomnyashchii, A. B.; Bröring, M.; Ahrens, J.; Bard, A. J. *J. Am. Chem. Soc.* **2011**, *133*, 19498−19504.
(29) Benniston, A. C.; Harriman, A.; Whittle, V. L.; Zelzer, M.; Harrington, R. W.; Clegg, W. *Photochem. Photobiol. Sci.* **2010**, *9*, 1009−1017.
(30) Nepomnyashchii, A. B.; Bard, A. J. *Acc. Chem. Res.* **2012**, *45*, 1844−1853.
(31) Granovsky, A. A. *J. Chem. Phys.* **2011**, *134*, 214113.
(32) Momeni, M. R.; Brown, A. *J. Chem. Theory Comput.* **2015**, *11*, 2619−2632.
(33) Charaf-Eddin, A.; Le Guennic, B.; Jacquemin, D. *RSC Adv.* **2014**, *4*, 49449−49456.
(34) Stromeck-Faderl, A.; Pentlehner, D.; Kensy, U.; Dick, B. *ChemPhysChem* **2011**, *12*, 1969−1980.
(35) Bergström, F.; Mikhalyov, I.; Hägglöf, P.; Wortmann, R.; Ny, T.; Johansson, L. B. Å. *J. Am. Chem. Soc.* **2002**, *124*, 196−204.
(36) Dähne, S. *Science* **1978**, *199*, 1163.
(37) Hanson, K.; Roskop, L.; Djurovich, P. I.; Zahariev, F.; Gordon, M. S.; Thompson, M. E. *J. Am. Chem. Soc.* **2010**, *132*, 16247−16255.
(38) Nijegorodov, N.; Winkoun, D. P. *Spectrochim. Acta, Part A* **1997**, *53*, 2013−2022.
(39) Turro, N. J.; Ramamurthy, V.; Scaiano, J. C. *Principles of Molecular Photochemistry: An Introduction*; University Science Books: Sausalito, California, 2009.
(40) Granovsky, A. A. *J. Chem. Phys.* **2011**, *134*, 214113.
(41) Granovsky, A. A. *Firefly version 8*; http://classic.chem.msu.su/gran/firefly/index.html.

DOI: 10.1021/acs.joc.7b00786
J. Org. Chem. 2017, 82, 7215−7222